International Journal of Nanomedicine

Dovepress
Taylor & Francis Group

Open Access Full Text Article

ORIGINAL RESEARCH

Clustered, SERS-Active, Ultrasmall AuNPs for Photothermal Therapy

Ryan D Mellor[1], Guojun Xiong[1], Alexandra G Vaideanu[1], Benjamin Gardner[2], Nick Stone[2], Andreas G Schätzlein[1], Ijeoma F Uchegbu[1]

[1]School of Pharmacy, University College London (UCL), London, WC1N 1AX, UK; [2]School of Physics and Astronomy, University of Exeter, Exeter, EX4 4QL, UK

Correspondence: Ijeoma F Uchegbu, School of Pharmacy, University College London (UCL), 29–39 Brunswick Square, London, Tel + 44 207 753 5997, Email ijeoma.uchegbu@ucl.ac.uk

Introduction: Gold nanoclusters (AuNCs) have emerged as promising agents for photothermal cancer therapy due to their unique optical properties and potential for tumour targeting.

Methods: In this study, we developed clustered, excretable AuNCs using a glycol chitosan derivative (GCPQ) and investigated their physicochemical properties, photothermal effect, and therapeutic efficacy.

Results: The AuNCs exhibited tunable surface plasmon resonance peaks dependent on the polymer:AuNP ratio, with optimized clusters showing surface enhanced Raman scattering and photothermal heating. In vivo studies in a mouse tumour model demonstrated significant tumour growth inhibition (334% growth vs 607% growth for untreated animals after 6 days) when combining intratumoural AuNC injection with near-infrared laser irradiation.

Conclusion: The results provide proof-of-concept for the potential of these AuNCs in photothermal cancer therapy. Future work should focus on improving tumour targeting, optimizing treatment parameters, and assessing long-term safety to advance this platform toward clinical translation.

Keywords: gold nanoclusters, (AuNCs), cancer treatment, glycol chitosan derivative, (GCPQ), tumour growth inhibition

Introduction

Photothermal therapy (PTT) is a promising approach for the treatment of cancer that utilizes the conversion of light into heat to selectively ablate tumour cells.[1] The approach relies on the use of photothermal agents that can efficiently convert light into heat, leading to localized hyperthermia and tumour cell death.[2,3] Additionally, the treatment is minimally invasive as it can be performed using external light sources, such as lasers, which can be precisely targeted to the tumour site.[4]

Gold nanoparticles (AuNPs) have attracted significant interest in recent years due to their unique physicochemical properties, including their size- and shape-dependent optical properties, biocompatibility, and ease of functionalization.[5] These properties make AuNPs promising candidates for a wide range of applications, including drug delivery, imaging, and photothermal therapy.[6] Additionally, AuNPs exhibit surface-enhanced Raman scattering (SERS) properties, which can be exploited for non-invasive detection of the particles in biological samples.[7] However, the clinical translation of AuNPs for photothermal therapy has been limited by challenges such as poor tumour accumulation, potential long-term toxicity, and the need for active targeting strategies to enhance therapeutic efficacy.[8]

Gold nanoparticles exhibit SERS properties due to their ability to enhance the local electromagnetic field when excited by light at their surface plasmon resonance frequency.[9] This enhancement occurs primarily at the surface of the nanoparticles and in small gaps between them (hotspots), leading to a significant increase in Raman scattering intensity from molecules adsorbed on or near the nanoparticle surface.[10] This phenomenon makes AuNPs excellent candidates for sensitive molecular detection in biological systems.[11]

Gold nanoclusters (AuNCs), also referred to as ultrasmall-in-nano constructs, represent a promising platform for photothermal therapy due to their enhanced photothermal properties compared to individual AuNPs.[12–14] The clustering

Received: 24 December 2024
Accepted: 29 April 2025
Published: 25 June 2025

of AuNPs can lead to a red shift in the surface plasmon resonance (SPR) peak,[15,16] resulting in increased light absorption and heat generation. Furthermore, the utilisation of gold building blocks of a size smaller that the limit for glomerular filtration, suggest potential feasibility of rapid excretion, if clusters can disassemble.

The clustering of AuNPs into AuNCs leads to enhanced photothermal properties through several mechanisms. Firstly, the close proximity of individual AuNPs within a cluster allows for plasmonic coupling, which can result in a red-shift and broadening of the surface plasmon resonance band.[17] This shift allows for better overlap with near-infrared light typically used in photothermal therapy, improving light absorption and heat generation.[18] Secondly, the clustered structure can create "hot spots" where the electromagnetic field is particularly intense, further enhancing light absorption and heat generation, if the illuminating light is resonant with the surface plasmon of the cluster.[19] Lastly, the larger overall size of AuNCs compared to individual AuNPs can lead to longer retention times in tumours due to the enhanced permeability and retention (EPR) effect, potentially improving therapeutic efficacy.[20]

Additionally, the SERS capabilities of gold nano constructs can be leveraged for advanced applications such as T-SESORS (Temperature-dependent Surface-Enhanced Spatially Offset Raman Spectroscopy).[21] This emerging technology allows for real-time, non-invasive temperature monitoring during photothermal therapy by combining deep tissue penetration with temperature-sensitive Raman reporters. The integration of T-SESORS with AuNCs could enable precise control and optimization of the photothermal effect, potentially enhancing treatment efficacy while minimizing damage to surrounding healthy tissues.

Furthermore, the use of biocompatible polymers to cluster the AuNPs can improve their stability, biocompatibility, and potential for active targeting.[22] In this study, we synthesized clustered AuNCs using a glycol chitosan derivative (GCPQ)[23] and investigated their physicochemical properties, photothermal effect, and therapeutic efficacy in a mouse tumour model.

Despite these promising characteristics, several challenges remain in the development of AuNCs for effective photothermal therapy. These include optimizing the balance between cluster size and tumour penetration, ensuring sufficient tumour accumulation, and minimizing potential long-term toxicity.[24] Additionally, the excretion pathway and long-term fate of AuNCs in biological systems are not fully understood.[25]

The aim of this study is to address these challenges by developing and characterizing a novel AuNC system using a glycol chitosan derivative (GCPQ) as a clustering agent. Specifically, we seek to synthesize and characterise GCPQ-clustered AuNCs with tunable physicochemical properties and to evaluate the in vivo photothermal therapy efficacy of the AuNCs in a mouse tumour model. By addressing these objectives, we aim to advance the development of AuNCs as a promising platform for photothermal cancer therapy, providing insights into their behaviour in biological systems and paving the way for future clinical translation.[26]

Materials and Methods

This study aimed to develop and characterize gold nanoclusters (AuNCs) for photothermal cancer therapy through a three-stage synthesis process. First, hydrophobic ultrasmall gold nanoparticles were synthesized via reduction of tetrachloroauric acid using sodium borohydride in the presence of biphenyl-4-thiol (which served dual purposes as a hydrophobic capping agent for subsequent clustering and as a Raman reporter molecule) and tetraoctylammonium bromide as a phase transfer agent. Second, a glycol chitosan derivative (GCPQ) polymer was prepared through acid hydrolysis of glycol chitosan to reduce molecular weight, followed by palmitoylation to introduce hydrophobic domains and quaternization reactions to enhance aqueous solubility and cellular interactions. Finally, the AuNCs were formed by clustering the hydrophobic nanoparticles using GCPQ polymer through a process of sonication, solvent evaporation, and aqueous redispersion, with investigation of various polymer:AuNP ratios to optimize the clustering process and resultant optical properties.

All experiments were conducted at room temperature (20–25°C) unless otherwise stated, using reagents as received. All glassware involved in AuNP synthesis was cleaned with aqua regia and thoroughly rinsed with deionized water before use. A table of materials used in this study can be found in Supplementary Table 1.

Particle Synthesis

Hydrophobic Ultrasmall AuNPs

Hydrophobic ultrasmall gold nanoparticles (AuNPs) were synthesised according to literature methods[27] with minor modifications. Under vigorous stirring, the following solutions were combined with 5 minutes between each addition, tetrachloroauric (III) acid trihydrate ($HAuCl_4 \cdot 3H_2O$, 25 mM, H_2O, 20 mL), tetraoctylammonium bromide (TOAB, 75 mM, toluene, 20 mL), biphenyl-4-thiol (BPT, 50 mM, toluene, 20 mL), and sodium borohydride ($NaBH_4$, 250 mM, H_2O, 20 mL) added dropwise. Stirring continued for 2 hours, after which the aqueous layer was discarded. The organic layer was washed three times (H_2O, 30 mL) and concentrated using a rotary evaporator to ~ 1 mL on a RV 10 Digital (IKA, Staufen, Germany). The particles were collected by precipitation (ethanol, 50 mL, 4°C, 16 hours), centrifugation (2.3×10^3 rpm (~1×10^3 rcf), 10 minutes), using a Sigma 3–16KL centrifuge (Swing-out rotor 11180, Round bucket 13190, Sigma, Osterode am Harz, Germany) and washed (ethanol, 50 mL) before being dried *in vacuo* to yield the final product (dark blue powder, 133.6 mg).

GCPQ Polymer

GCPQ polymer was synthesised as previously reported[28,29] with minor modifications. Glycol chitosan (GC, 30 g) was degraded by hydrochloric acid catalysed hydrolysis (4 M HCl, 200 mL, 50°C, 24 hours) with vigorous stirring, followed by precipitation (acetone, 750 mL), trituration (acetone, 3×150 mL collection using a sintered glass filter, and drying using a rotary evaporator. Under vigorous stirring, degraded glycol chitosan (dGC, 30 g) was dispersed (5% v/v TEA/DMSO, 300 mL) followed by the addition of palmitic acid N-hydroxysuccinimide ester (PNS, 11.57 g), and the reaction continued with stirring (dark, room temperature, 16 hours). The product was collected by precipitation (33% v/v acetone/diethyl ether, 1.35 L), trituration (acetone 3×260 mL, and diethyl ether 3×260 mL), and drying using a rotary evaporator. Under vigorous stirring and nitrogen atmosphere, palmitoyl glycol chitosan (pGC, 30 g) was dispersed in N-methyl-2-pyrrolidone (NMP, 1.75 L) followed by the addition of sodium hydroxide (NaOH, 4.067 g, dispersed in NMP, 500 mL), sodium iodide (NaI, 4.619 g, dispersed in NMP, 250 mL), and methyl iodide (MeI, 45 mL), the reaction continued with stirring under a sealed nitrogen atmosphere (37 °C, 1 hour). The product was collected by precipitation (aqueous 100 mM NaOH, 7.5 L), centrifugation (4×10^3 rpm (~3×10^3 rcf), 5 minutes), redispersion (H_2O, 600 mL), pH adjustment to pH = 3–4 with HCl (10.2 M), dialysis against H_2O (12×5 L, 48 hours, MWCO 3.5 kDa), and freeze drying using a ALPHA 1–4 LDplus (Christ, Germany).

Clusters

Gold nanoclusters (AuNCs) were synthesised by clustering hydrophobic ultrasmall particles using GCPQ polymer. To a dispersion of GCPQ (1 mg/mL, ethanol, 500 µL, filtered 0.2 µm) was added a dispersion of AuNPs (10 mg/mL, chloroform, 1 mL) followed by bath sonication (5 minutes), rotary evaporation of solvent, redispersion (H_2O, 25 mL), bath sonication (5 minutes), probe sonication (5 amp, 3×5 minutes on 5 minutes off, on ice) using a Soniprep 150 plus (MSE, Crowley, UK), and dilution (H_2O, 25 mL). The gold nano clusters (AuNCs) were collected by centrifugation (3×10^3 rpm (~1.7×10^3 rcf), 10 minutes), removal of supernatant, and the volume was made up to 2 mL with H_2O.

Effect of Polymer: AuNP Ratio on Clusters

The effect of varying the polymer: AuNP ratio was investigated. Following the protocol above, various volumes of GCPQ dispersion were used (1 mg/mL, 15, 30, 150, 300, 1500, and 3000 µL), and all other volumes scaled proportionally with respect to the volume of the AuNP dispersion used (50 µL). The speed of centrifugation was increased to 1×10^4 rpm (~1.9×10^4 rcf) to pellet the smallest particles, ie those produced with 1500 and 3000 µL of GCPQ dispersion.

Particle Characterization

Transmission Electron Microscopy

Transmission Electron Microscopy (TEM) images were recorded using a JEM-1400 Flash Electron Microscope (JEOL, Tokyo, Japan) with a Gatan Rio CMOS camera at an accelerating voltage of 120kV. Samples were prepared by drop

casting a dilute dispersion of the particles onto a formvar/carbon film on copper 300 mesh (EM Resolutions, UK) and allowing the sample to dry under ambient conditions. Particle size and count were determined using ImageJ software.

UV-Vis Spectroscopy

Extinction spectra were recorded using a GENESYS 50 UV-Vis spectrophotometer (Thermo Scientific, Waltham, MA, USA) using a disposable cuvette (1 cm path length). The spectra were normalised to the extinction at 450 nm, a surrogate measure for an approximation of gold concentration, to allow for comparison between samples. The position of the Surface Plasmon Resonance (SPR) peak was determined as the wavelength of maximum extinction.

Dynamic Light Scattering

Dynamic light scattering (DLS) measurements were performed on 10× diluted aqueous samples in plastic cuvettes at room temperature (25 °C), with the viscosity set to that of water. Refractive index and absorption were set to 0.20 and 3.32, respectively.[30] Measurements were performed on a Zetasizer Ultra (Malvern Panalytical, Malvern, UK) at least 3 times, and the average is reported.

Raman Spectroscopy

Raman spectroscopy measurements were conducted on aqueous dispersions of particles (5 µL, ~1 mg/mL AuNC). Spectra were recorded using a Raman system comprised of a 785 nm digital multi-mode spectrum-stabilized laser module (I0785MM0350MF-USB, IPS, Compton, CA, USA), a 785 nm high throughput probe (I0785P-FS-32-125-08, IPS, Compton, CA, USA), and a 750–1050 nm high performance smart spectrometer with a thermoelectric, cooled back-thinned CCD and a 25 µm slit (BTC655N, B&W Tek, Newark, DE, USA). The laser power was set to 100 mW, and the spectra were recorded in the range 200–2000 cm^{-1} with an integration time of 10 seconds.

Laser Induced Heating

In vitro laser-induced heating experiments were performed using an 808 nm laser set to 100 mW for 5 minutes and focused onto a sample of the AuNC dispersion (50 µL) in an Eppendorf tube. The temperature change was monitored using the photothermal apparatus and software described below.

Construction of Photothermal Apparatus

The optics of the photothermal apparatus consist of a laser module (808 nm, 500 mW, I0808MM0500MF-USB, IPS, Compton, CA, USA) coupled to a collimating lens (F220FC-780, Thorlabs, NJ, USA) via fibre optic. The apparatus was constructed such that the open beam is inside an opaque enclosure. Within the enclosure is a thermal imaging camera (CompactPro, Seek Thermal, USA), low profile anaesthesia facemask (Kent Scientific), a heat mat (5W, 6×5.5 inches), and a thermocouple probe (USB-2001-TC, Measurement Computing, MA, USA) (Figure 1). The collimated laser beam produced by the apparatus was characterised using a beam profiler and found to have a beam diameter of ~3 mm.

The use of a thermocouple probe allows for the calibration of the thermal imaging camera, which is necessary for accurate temperature measurements as the camera does not provide absolute temperature readings. The camera was calibrated by aligning the thermocouple probe with the centre of the camera's field of view and recording the temperature readings from both devices simultaneously for ambient (~25°C) and with the heat mat at full power (~45°C). The calibration was performed using a linear regression of the thermocouple readings against the camera readings.

Development of Control and Analysis Software

Custom control and analysis software was developed using the programming language Python, the graphical user interface was predominantly written using the libraries PyQt5[31] and PyQtGraph.[32] Key features of the software include capture of images and video, one- and two-point camera calibration against a thermocouple, and region of interest analysis both during capture and for loaded data (Figure 2).

The software is freely available for download at https://github.com/RyanMellor/ThermalImaging.

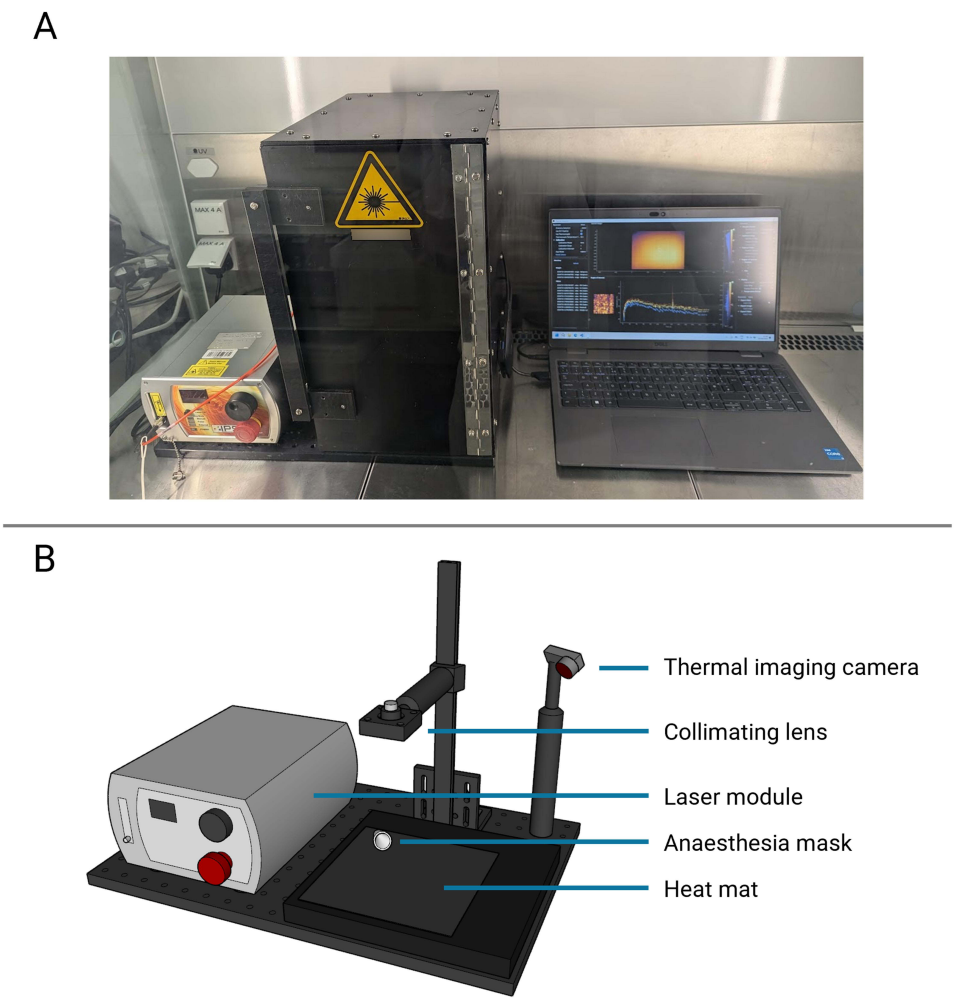

Figure 1 Photothermal therapy apparatus. Photograph in situ (**A**) and labelled schematic (**B**).

Photothermal Therapy

Tumours were established by subcutaneous injection of 2×10^6 4T1 cells (ATCC, UK) into the right flank of female BALB/c mice (8 weeks at the time of injection), 5 mice were used per treatment group. Tumours were monitored every two days until a tumour volume of approximately 100 mm^3 was reached, at which point a volume of sample (20–50 µL) proportional to the tumour volume was injected intratumourally. After at least 1 hour post injection, the mice were anaesthetised using isoflurane and loaded into the photothermal therapy apparatus where they remained under anaesthesia for the duration of the experiment. Tumours were aligned with the laser beam and irradiated at 4.5 W/cm^2 for 10 minutes. Control groups included AuNC injection without subsequent laser irradiation, and saline injection both with and without laser irradiation.Tumour width and length, and body weights were recorded daily, and tumour volumes were calculated according to the following equation:

$$V = 0.5 \times L \times W^2$$

Where V = tumour volume, L = tumour length, and W = tumour width.

The animal experiments were performed under a UK Home Office Licence in accordance with the Animal Scientific Procedures Act 1986. All experiments were approved by the UCL Animal Welfare and Ethical Review Body.

https://doi.org/10.2147/IJN.S513400

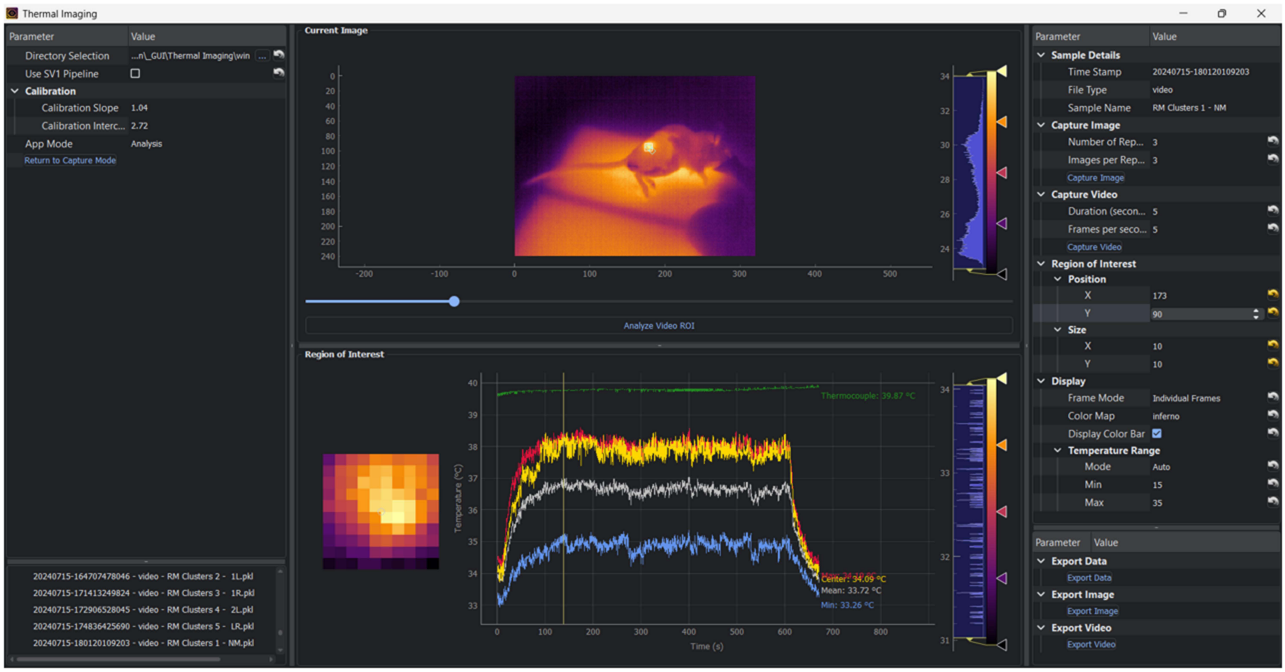

Figure 2 Graphical user interface for photothermal apparatus control and analysis software.

Results and Discussion

Particle Synthesis and Characterization

Hydrophobic ultrasmall gold nanoparticles (AuNPs) were synthesised using a modified Brust-Schiffrin method,[27,33] and gold nanoclusters (AuNCs) were formed by clustering the AuNPs with GCPQ polymer, which has previously been used to encapsulate pre-formed gold nano clusters.[15] AuNPs were characterised by Transmission Electron Microscopy (TEM), and AuNCs were characterised by UV-Vis spectroscopy, Raman spectroscopy, and laser-induced heating experiments. The effect of varying the polymer: AuNP ratio on the physicochemical properties of the AuNCs was investigated, and the optimal conditions were determined. In vivo photothermal therapy experiments, following intratumoural injection, were performed to assess the therapeutic efficacy of the AuNCs, and the biodistribution of the AuNCs following intravenous injection was quantified to determine their accumulation in key organs and the tumour.

Hydrophobic Ultrasmall AuNPs

Figure 3 shows the TEM image and size distribution of the hydrophobic ultrasmall AuNPs. The particles are quasi-spherical with an average diameter of 2.37 ± 0.91 nm (n=1193). The hydrophobic coating of BPT ensures the stability of the AuNPs in organic solvents and facilitates the clustering process with the GCPQ polymer.

The SPR peak of the AuNCs was found to be dependent on the polymer: AuNP ratio, as shown in Figure 4A. The optimal conditions for the synthesis of AuNCs were determined to be a polymer: AuNP ratio of 0.03:1 (Figure 4B). The Raman spectrum of the AuNCs exhibited characteristic peaks of biphenyl-4-thiol (BPT), confirming the presence of the hydrophobic ligand on the surface of the AuNCs (Figure 4C), in particular the peak at 1589 cm^{-1} was used to quantify Raman intensity.

Clusters

The variation in the SPR peak position is attributed to the decrease in average size of the AuNC with increasing polymer: AuNP ratio, as shown in Figure 5 as the localised surface plasmon resonance of the AuNCs is known to be a size-dependent property.

The effect of the position of the SPR peak on the physicochemical properties of the AuNCs was investigated, as shown in Figure 6. The Raman intensity of the AuNCs was found to be dependent on the position of the SPR peak, with

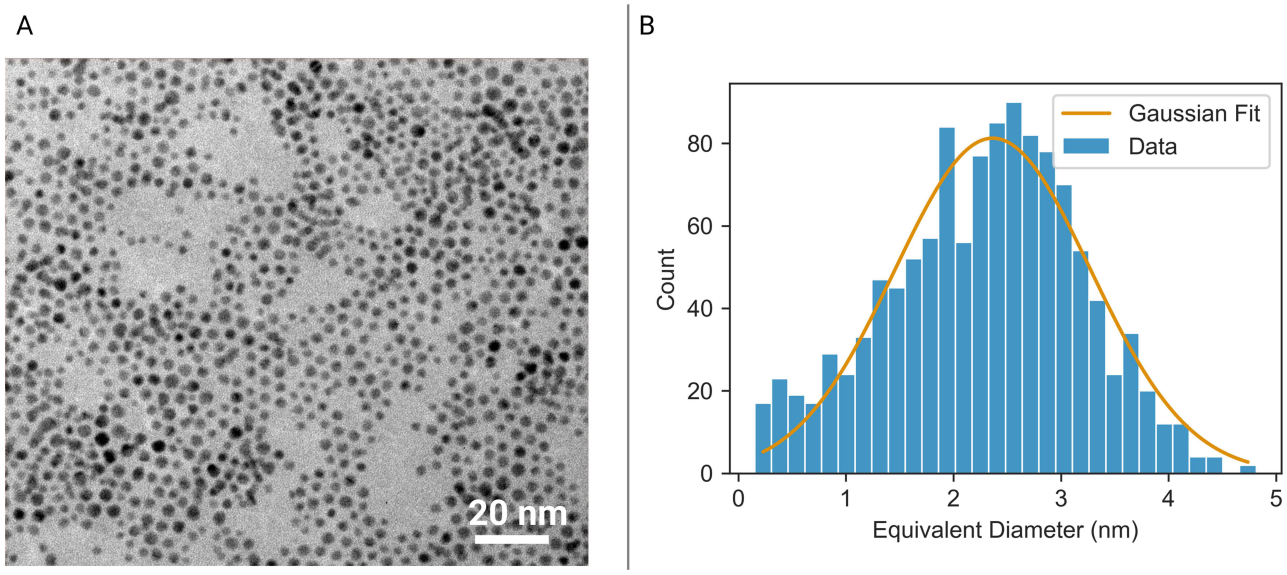

Figure 3 Hydrophobic BPT-coated AuNPs. Transmission Electron Microscopy (TEM) image (**A**) and size distribution (**B**).

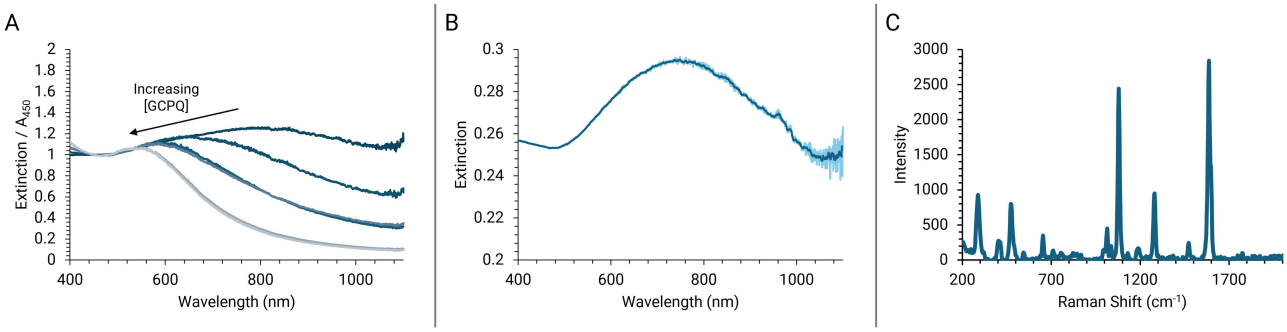

Figure 4 Spectroscopic characterization of AuNCs. Extinction spectra with varying Polymer: AuNP ratio (**A**, normalised by A_{450}), optimised synthesis conditions (**B**), and Raman spectra (**C**).

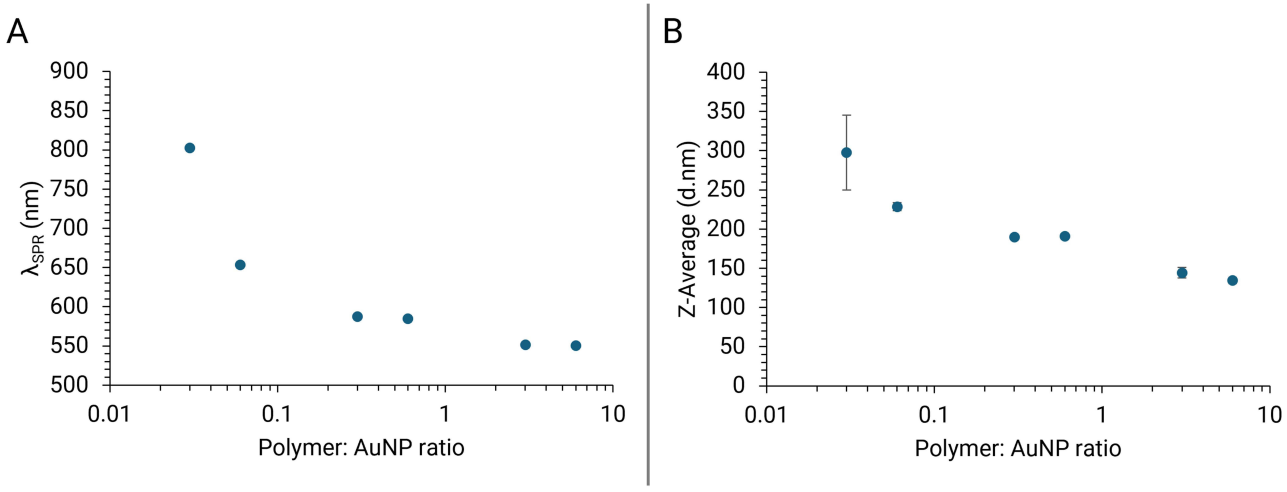

Figure 5 Effect of varying polymer: AuNP ratio on physicochemical properties of AuNC. Position of Surface Plasmon Resonance (SPR) peak (**A**), and Z-average hydrodynamic diameter (**B**).

https://doi.org/10.2147/IJN.S513400

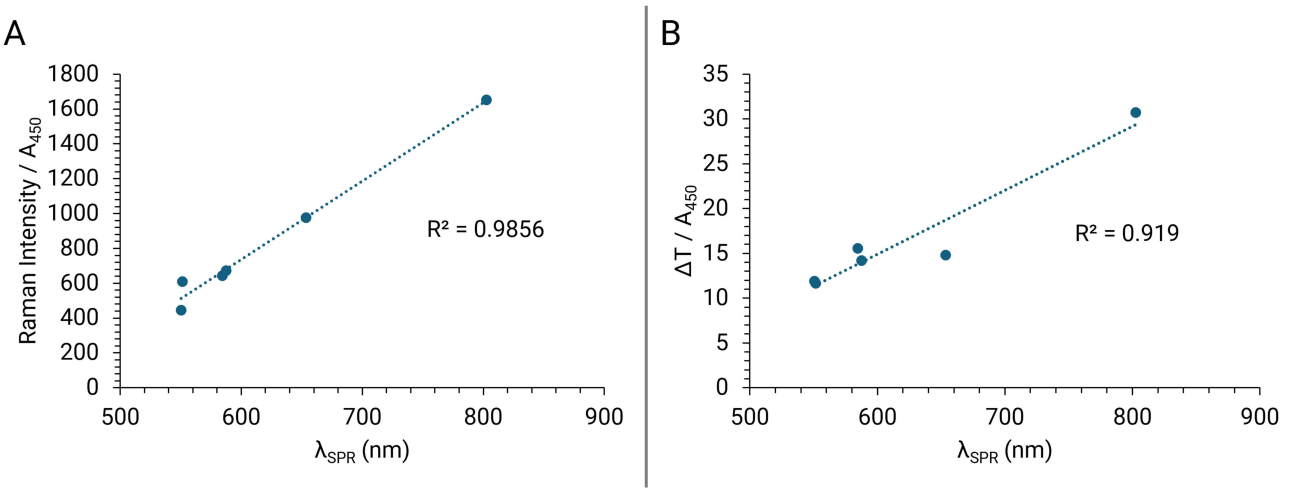

Figure 6 Effect of position of Surface Plasmon Resonance (**A**) peak on physicochemical properties of AuNC. Raman intensity (left), and temperature change upon laser induced heating (**B**).

a red-shifted peak resulting in increased Raman intensity. The temperature change upon laser-induced heating was also found to be dependent on the position of the SPR peak. When the surface plasmon resonance in the AuNCs is red-shifted to become resonant and more absorbing at the laser wavelength of 808 nm, this results in a greater and more rapid temperature increase. These results demonstrate that the position of the SPR peak can be tuned to optimise the photothermal properties of the AuNCs for therapeutic applications, for a specific laser wavelength. Furthermore, shifting the LSPR towards the laser line increases the electric field generated in the cluster hotspots, resulting in a higher Raman scattered signal from the reporter labels residing in the hotspots.

Under forced degradation testing conditions,[34] AuNCs were found to have good aqueous stability at 40 °C with minimal change in extinction spectra for the duration of the study (Supplementary Figure 1). The photothermal data of the optimized clusters is demonstrated by temperature curve and photothermal imagery time course in Supplementary Figure 2.

Photothermal Therapy

The photothermal effect and therapeutic efficacy of the gold nanoclusters were investigated in vivo. The ability of the nanoclusters to generate heat upon laser irradiation and the resulting impact on tumour growth were assessed to determine the potential of this platform for photothermal cancer therapy.

Figure 7 illustrates the change in temperature over time for the gold nanoclusters, as well as a saline control. The saline control (orange curve) showed minimal temperature changes, with increases of less than 2°C over the 10 minutes of laser irradiation. However, the clusters (blue curve) demonstrated a notable temperature increase of approximately 5°C on average and as much as 7.5°C. This suggests that while the laser irradiation alone does not generate significant heat, there is a significantly enhanced photothermal response when combined with intratumoural injection of gold nanoclusters.

The observed temperature change for the laser irradiated clusters in vivo (5°C at 4.5 W/cm^2) is relatively low compared to the temperature increase observed in vitro (31°C at 1.5mW/cm^2). This is due to several contributing factors. Performing experiments in vivo results in significant loss of laser photons due to their scattering by skin and tissues surrounding the AUNCs, whereas the AUNCs in vitro are in a relatively low scattering environment. Furthermore, in perfused tissues there will be a reduction in overall heating due to the competing effect of homeostatic thermoregulatory systems of the organism.[35] Furthermore, temperature readings in vivo are only a surface measurement and so the centre of the tumour is likely to be hotter as the heat radiates from the AuNCs.

The in vivo therapeutic efficacy of the photothermal treatment was assessed in a mouse tumour model, as presented in Figure 8. Tumour growth was monitored for up to 8 days post-treatment when the clusters were administered via the

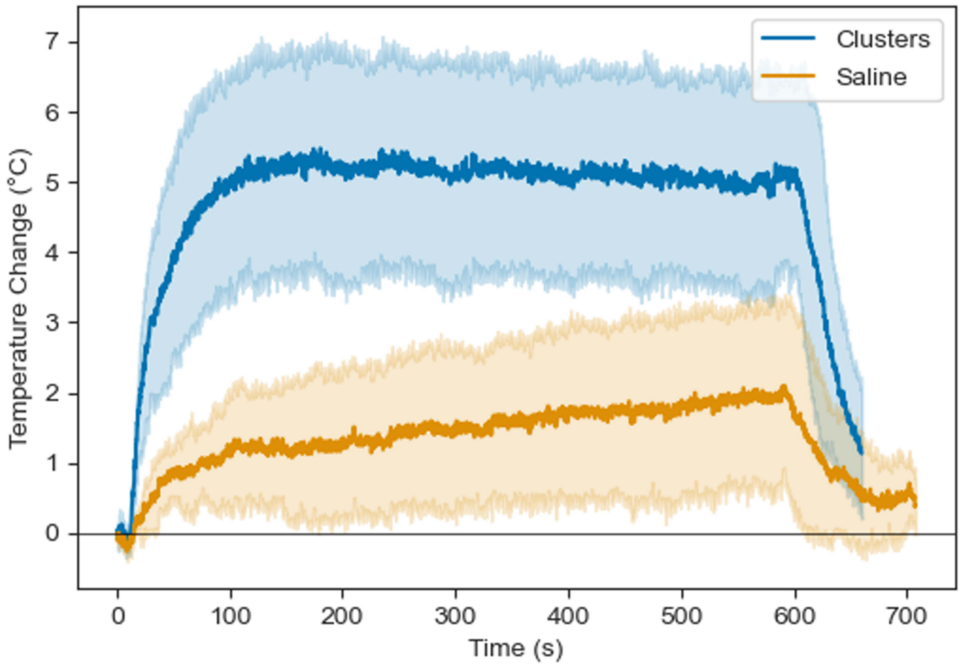

Figure 7 Temperature of tumour (ROI centre) during photothermal therapy experiments.

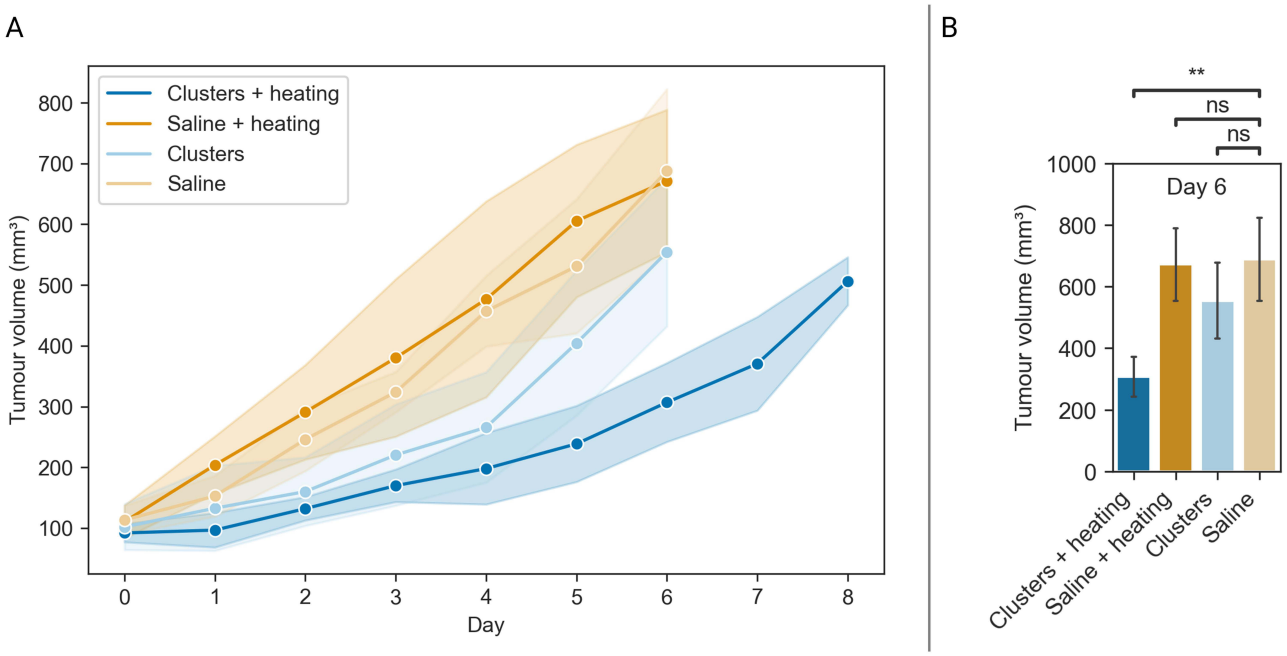

Figure 8 Effect of photothermal therapy on rate of tumour progression, full time course (**A**) and comparison at day 6 (**B**) – the last time point with data available for all groups. $*0.001 < p \leq 0.05$; $***0.0001 < p \leq 0.001$.

intratumoural route; however, most tumours exceeded the humane limit (500 mm^3) after just 6 days. For each group, the body weight remained constant over the course of the study (Supplementary Figure 3).

Statistical analysis was performed to compare the rate of tumour growth between the different treatment groups, significance was determined using ANOVA with Tukey posthoc (Figure 8). Only the combination of 'Clusters + heating' demonstrated a statistically significant difference compared to all other test groups (p=0.001 vs 'Saline + heating',

https://doi.org/10.2147/IJN.S513400

p=0.002 vs 'Clusters', and p=0.001 vs 'Saline') in the rate of tumour growth after 6 days (the last timepoint with data available for all groups). This highlights the importance of the synergistic effect between the gold nanoclusters and external heating for achieving effective tumour growth inhibition.

Conclusion

The gold nanoclusters (AuNCs) developed in this study demonstrated significant potential for photothermal therapy applications in cancer treatment. Our findings contribute to the growing body of evidence supporting the use of nanoparticle-based approaches in cancer theranostics. We successfully developed a method to synthesize GCPQ-clustered AuNCs with tunable physicochemical properties, providing a versatile platform for optimizing photothermal performance. The ability to control the surface plasmon resonance peak position through adjusting the polymer:AuNP ratio is particularly noteworthy.

Our in vivo studies demonstrated a significant photothermal effect when the AuNCs were non-invasively irradiated with laser light at 808 nm; leading to enhanced tumour growth inhibition compared to the controls. This proof-of-concept validates the potential of our AuNC system for photothermal therapy applications.

However, it is crucial to acknowledge the limitations of our study. While the treatment with AuNCs plus laser irradiation significantly inhibited tumour growth, complete tumour elimination was not achieved. This underscores the need for optimization of treatment parameters, which may include repeated treatments or potential combinational therapies. Long-term safety studies are needed to fully assess the potential toxicity and ultimate fate of these nanoparticles in biological systems.

To address these limitations and further improve the efficacy of the treatment, several avenues can be explored. Incorporating tumour-specific ligands or antibodies onto the AuNC surface could enhance therapeutic efficacy. This could be easily achieved due to the use of a readily modifiable polymer coating. The treatment regimen could be optimized by increasing the number, duration, and/or power of the photothermal therapy sessions. Additionally, increasing the spot size of the laser while maintaining power density may lead to a more effective treatment, as the current spot size was significantly smaller than the tumour itself.

Exploring the synergistic effects of combining photothermal therapy with other treatment modalities, such as chemotherapy or immunotherapy, may lead to more robust anti-tumour responses. Comprehensive evaluation of the long-term safety of AuNCs is essential for clinical translation. Moreover, further development of the SERS capabilities of our AuNCs could enable their use as both therapeutic and diagnostic agents, allowing for real-time monitoring of treatment response.

In conclusion, our GCPQ-clustered AuNC system represents a promising platform for photothermal cancer therapy. The tunability of their physicochemical properties, combined with their photothermal efficacy, provides a solid foundation for further development. While the single treatment was not able to eliminate the tumour completely, this study serves as a promising proof of concept. By addressing the identified limitations and pursuing the suggested future directions, we believe that this approach has the potential to significantly impact the field of nanoparticle-based cancer theranostics and move closer to clinical application.

Acknowledgments

This research was funded by UK Engineering and Physical Sciences Research Council, grant number EP/R020965/1. The APC was funded by EP/R020965/1.

Disclosure

AGS is the CEO of Nanomerics Ltd who have a license from University College London for related polymer technology. The authors report no other conflicts of interest in this work.

References

1. Jaque D, Martínez Maestro L, Del Rosal B, et al. Nanoparticles for photothermal therapies. *Nanoscale*. 2014;6(16):9494–9530. doi:10.1039/C4NR00708E

2. Huang X, Jain PK, El-Sayed IH, El-Sayed MA. Plasmonic photothermal therapy (PPTT) using gold nanoparticles. *Lasers Med Sci*. 2008;23(3):217–228. Available from: https://link.springer.com/article/10.1007/s10103-007-0470-x. Accessed August 8, 2024.
3. Abadeer NS, Murphy CJ. Recent progress in cancer thermal therapy using gold nanoparticles. *J Phys Chem C*. 2016;120(9):4691–4716. doi:10.1021/acs.jpcc.5b11232
4. Huang X, El-Sayed IH, Qian W, El-Sayed MA. Cancer cell imaging and photothermal therapy in the near-infrared region by using gold nanorods. *J Am Chem Soc*. 2006;128(6):2115–2120. doi:10.1021/ja057254a
5. Daniel MC, Astruc D. Gold nanoparticles: assembly, supramolecular chemistry, quantum-size-related properties, and applications toward biology, catalysis, and nanotechnology. *Chem Rev*. 2004;104(1):293–346.
6. Dreaden EC, Alkilany AM, Huang X, Murphy CJ, El-Sayed MA. The golden age: gold nanoparticles for biomedicine. *Chem Soc Rev*. 2012;41(7):2740–2779. doi:10.1039/C1CS15237H
7. Qian X, Peng XH, Ansari DO, et al. In vivo tumor targeting and spectroscopic detection with surface-enhanced Raman nanoparticle tags. *Nat Biotechnol*. 2008;26(1):83–90. doi:10.1038/nbt1377
8. Pedrosa P, Vinhas R, Fernandes A, Baptista PV. Gold nanotheranostics: proof-of-concept or clinical tool? *Nanomaterials*. 2015;5(4):1853–1879. doi:10.3390/nano5041853
9. Schlücker S. Surface-enhanced raman spectroscopy: concepts and chemical applications. *Angewandte Chemie Int Edition*. 2014;53(19):4756–4795. doi:10.1002/anie.201205748
10. Stiles PL, Dieringer JA, Shah NC, Van Duyne RP. Surface-enhanced raman spectroscopy. *Annual Rev Anal Chem*. 2008;1(1):601–626. doi:10.1146/annurev.anchem.1.031207.112814
11. Kneipp J, Kneipp H, Kneipp K. SERS—a single-molecule and nanoscale tool for bioanalytics. *Chem Soc Rev*. 2008;37(5):1052. doi:10.1039/b708459p
12. Rengan AK, Bukhari AB, Pradhan A, et al. In vivo analysis of biodegradable liposome gold nanoparticles as efficient agents for photothermal therapy of cancer. *Nano Lett*. 2015;15(2):842–848. doi:10.1021/nl5045378
13. Cassano D, Santi M, D'Autilia F, Katrina Mapanao A, Luin S, Voliani V. Photothermal effect by NIR-responsive excretable ultrasmall-in-nano architectures. *Mat Horizons*. 2019;6(3):531–537. doi:10.1039/C9MH00096H
14. Deng H, Dai F, Ma G, Zhang X. Theranostic gold nanomicelles made from biocompatible comb-like polymers for thermochemotherapy and multifunctional imaging with rapid clearance. *Adv Mat*. 2015;27(24):3645–3653. doi:10.1002/adma.201501420
15. Mellor RD, Schätzlein AG, Uchegbu IF. Development of bio-functionalized, raman responsive, and potentially excretable gold nanoclusters. *Nanomaterials*. 2021;11(9):2181. doi:10.3390/nano11092181
16. Mellor RD, Uchegbu IF. Ultrasmall-in-Nano: why Size Matters. *Nanomaterials*. 2022;12(14):2476. doi:10.3390/nano12142476
17. Ghosh SK, Pal T. Interparticle coupling effect on the surface plasmon resonance of gold nanoparticles: from theory to applications. *Chem Rev*. 2007;107(11):4797–4862. doi:10.1021/cr0680282
18. Tabish TA, Dey P, Mosca S, et al. Smart gold nanostructures for light mediated cancer theranostics: combining optical diagnostics with photothermal therapy. *Adv Sci*. 2020;7(15):1903441. doi:10.1002/advs.201903441
19. Brongersma ML, Halas NJ, Nordlander P. Plasmon-induced hot carrier science and technology. *Nat Nanotech*. 2015;10(1):25–34. doi:10.1038/nnano.2014.311
20. Maeda H, Wu J, Sawa T, Matsumura Y, Hori K. Tumor vascular permeability and the EPR effect in macromolecular therapeutics: a review. *J Control Rel*. 2000;65(1–2):271–284. doi:10.1016/S0168-3659(99)00248-5
21. Gardner B, Matousek P, Stone N. Direct monitoring of light mediated hyperthermia induced within mammalian tissues using surface enhanced spatially offset Raman spectroscopy (T-SESORS). *Analyst*. 2019;144(11):3552–3555. doi:10.1039/C8AN02466A
22. Zhang L, Chan JM, Gu FX, et al. Self-assembled lipid−polymer hybrid nanoparticles: a robust drug delivery platform. *ACS Nano*. 2008;2(8):1696–1702. doi:10.1021/nn800275r
23. Chooi KW, Simão Carlos MI, Soundararajan R, et al. Physical characterisation and long-term stability studies on quaternary ammonium palmitoyl glycol chitosan (GCPQ)—A new drug delivery polymer. *J Pharmaceut Sci*. 2014;103(8):2296–2306. doi:10.1002/jps.24026
24. Wilhelm S, Tavares AJ, Dai Q, et al. Analysis of nanoparticle delivery to tumours. *Nat Rev Mater*. 2016;1(5):16014. doi:10.1038/natrevmats.2016.14
25. Longmire M, Choyke PL, Kobayashi H. Clearance properties of nano-sized particles and molecules as imaging agents: considerations and caveats. *Nanomedicine*. 2008;3(5):703–717. doi:10.2217/17435889.3.5.703
26. Vines JB, Yoon JH, Ryu NE, Lim DJ, Park H. Gold nanoparticles for photothermal cancer therapy. *Front Chem*. 2019;7:167. doi:10.3389/fchem.2019.00167
27. Heriot SY, Pedrosa JM, Camacho L, Richardson TH. Langmuir monolayer properties of 4-methylbenzenethiol capped gold nanoparticles. *Materials Science and Engineering: C*. 2006;26(1):154–162. doi:10.1016/j.msec.2005.08.001
28. Uchegbu IF, Sadiq L, Arastoo M, et al. Quaternary ammonium palmitoyl glycol chitosan—a new polysoap for drug delivery. *Int J Pharmaceut*. 2001;224(1–2):185–199. doi:10.1016/S0378-5173(01)00763-3
29. Lerchbammer-Kreith Y, Hejl M, Sommerfeld NS, et al. Quaternary ammonium palmitoyl glycol chitosan (GCPQ) loaded with platinum-based anticancer agents—A novel polymer formulation for anticancer therapy. *Pharmaceuticals*. 2023;16(7):1027. doi:10.3390/ph16071027
30. Gardiner C, Shaw M, Hole P, et al. Measurement of refractive index by nanoparticle tracking analysis reveals heterogeneity in extracellular vesicles. *J Extracell Vesicles*. 2014;3:25361. doi:10.3402/jev.v3.25361
31. Riverbank Computing | introduction. Available from: https://www.riverbankcomputing.com/software/pyqt/. Accessed August 8, 2024.
32. PyQtGraph. Scientific Graphics and GUI Library for Python. Available from: https://www.pyqtgraph.org/. Accessed August 8, 2024.
33. Brust M, Walker M, Bethell D, Schiffrin DJ, Whyman R. Synthesis of thiol-derivatised gold nanoparticles in a two-phase Liquid–Liquid system. *J Chem Soc Chem Commun*. 1994;(7):801–802. doi:10.1039/C39940000801
34. Blessy M, Patel RD, Prajapati PN, Agrawal YK. Development of forced degradation and stability indicating studies of drugs—A review. *J Pharmaceut Anal*. 2014;4(3):159–165. doi:10.1016/j.jpha.2013.09.003
35. Gordon CJ. The mouse thermoregulatory system: its impact on translating biomedical data to humans. *Physiol Behav*. 2017;179:55–66. doi:10.1016/j.physbeh.2017.05.026